Estimation of Surface Insolation Using Sun-Synchronous Satellite Data

WAYNE L. DARNELL AND W. FRANK STAYLOR

Atmospheric Sciences Division, NASA Langley Research Center, Hampton, Virginia

SHASHI K. GUPTA AND FRED M. DENN

PRC Kentron Inc., Hampton, Virginia

(Manuscript received 18 May 1987, in final form 25 April 1988)

ABSTRACT

A technique is presented for estimating insolation at the Earth's surface using only sun-synchronous satellite data. The technique was tested by comparing the insolation results from year-long satellite datasets with simultaneous ground-measured insolation taken at five continental United States sites. Monthly average insolation values derived from the satellite data showed a standard error of 4.2 W m^{-2}, or 2.7% of the average ground insolation value.

1. Introduction

Ground-based pyranometer measurements of incoming solar radiation (insolation) at the Earth's surface have been made at various land stations for many years. Such site measurements alone, however, cannot provide the spatial coverage needed for the important worldwide climate studies under way and planned. Global radiation monitoring must be done using satellite measurements. Tarpley (1979) used GOES (Geostationary Operational Environmental Satellite) VISSR (Visible and Infrared Spin Scan Radiometer) data to empirically estimate hourly and daily insolation over the United States Great Plains achieving about 10% accuracy. Gautier et al. (1980) also used GOES data, but with a columnar energy conservation model, to estimate daily insolation in southern Canada. This approach also provided accuracies of 10% for all-sky conditions. In later studies (Diak et al. 1982; Diak and Gautier 1983), the technique was improved and used in an ocean area. Pinker and Ewing (1985) tested and validated a technique using two ground datasets from the area of Toronto, Canada, and achieved accuracies of 12% and 18% for daily results. Justus et al. (1986) developed an insolation technique for producing 1° grid data over large areas of the United States, Mexico, and South America. The monthly means were accurate to about 5%. All of the foregoing investigators used geostationary satellite data for input to their models. This allowed them to take advantage of the inherent high temporal (1 h) and spatial (8 km) resolution of geostationary satellite radiance data. The disadvantage of this approach is that geostationary satellites do not permit global coverage. Interlocking combinations of datasets from three to five satellites must be obtained to provide complete longitudinal coverage, and zonally, coverage is limited to latitudes between 60°N and 60°S. A second problem is that each satellite sensor's response is slightly different. Difficult intercalibrations between the radiances of each satellite are required on a continuing basis. As a result, it has been desirable to have an insolation estimation technique that could use data from a single sun-synchronous satellite that would provide surface insolation estimations for the entire globe. While sun-synchronous satellites offer global coverage, they lack good temporal coverage since these satellites pass over most locations only once per day during daylight hours. Several sun-synchronous insolation techniques were developed earlier (e.g., Hanson 1971; Ellis and Vonder Haar 1978; Raschke and Preuss 1979) but these made extensive use of climatological values of meteorological data and were not developed sufficiently to be of operational use.

We present an insolation estimation technique based on a physical approach and which relies on data obtained from operational sun-synchronous satellites. The technique is designed for global use, but to illustrate the validation of the technique, 1-yr flux comparisons at five sites in the United States are presented herein since global surface datasets do not exist. This technique, along with an accompanying longwave technique based largely on the same input data, can provide an operational method for global study of the downwelling radiation fluxes at the surface.

Corresponding author address: Wayne Darnell, Atmospheric Sciences Division, NASA Langley Research Center, Mail Stop 420, Hampton, VA 23665-5225.

2. Ground truth and satellite data

Ground-measured insolation data were used to provide the groundtruth for development of the technique and for validating the satellite-estimated insolation values. Part of these data were provided by five university solar research centers, which operated continuously throughout the 1-yr data period (1 July 1981 through 30 June 1982). The data were taken from 1-min samplings by Eppley Precision Spectral Pyranometers and then converted to hourly insolation fluxes. The university sites were located at the University of California (CA), Davis, California; Georgia Institute of Technology (GA), Atlanta, Georgia; Hampton University (VA), Hampton, Virginia; University of Michigan (MI), Ann Arbor, Michigan; and State University of New York (NY), Albany, N.Y. In addition, long-term compilations of monthly, cloud-free insolation from the 26-station, SOLMET dataset (SOLMET 1979) were used for clear-sky validations. These stations are scattered throughout the United States, and the data covered the period from 1952 to 1976. The locations of these 26 sites (crosses) and the five university sites (solid circles) are shown in Fig. 1.

The purpose of selecting many different data sites and of an extended data period was to provide a very broad base for validation of the satellite technique. The 26-site NOAA dataset included very dry climates, coastal areas, mountainous areas, plains, and large cities. The five university sites were chosen because of their high data quality and because they had been used previously as validation points for earlier work concerning the development of a downward longwave model (Darnell et al. 1986).

Local meteorological data were used to compare the local surface meteorology with the broader-based satellite meteorology and to confirm the presence of totally clear-sky conditions or of snow cover at the sites. These data were from published *Local Climatological Data* available from the NOAA National Climatic Center, Asheville, North Carolina.

Satellite data consisted of Tiros Operational Vertical Sounder (TOVS) Meteorological Data Products and Advanced Very High Resolution Radiometer (AVHRR) Heat Budget Products obtained from the NOAA National Climatic Data Center, Washington, DC. These data were produced on an operational basis by NOAA from radiance measurements taken by the NOAA-6 and -7 satellites, which operated in sun-synchronous orbits with nominal equatorial crossing times of 0730/1930 and 0230/1430 local standard time (LST), respectively. The TOVS is a combination of three sounding instruments, but for this work, only data retrievals from the HIRS-2 (High resolution Infrared Sounder, Version 2) and from the MSU (Microwave Sounder Unit) are used. The TOVS has a nominal ground resolution, called a TOVS box, which covers about 3° × 3° at the Equator. From each of these boxes the following data products are retrieved: surface temperature, temperature profile, precipitable water vapor profile, cloud cover fraction, cloud-top

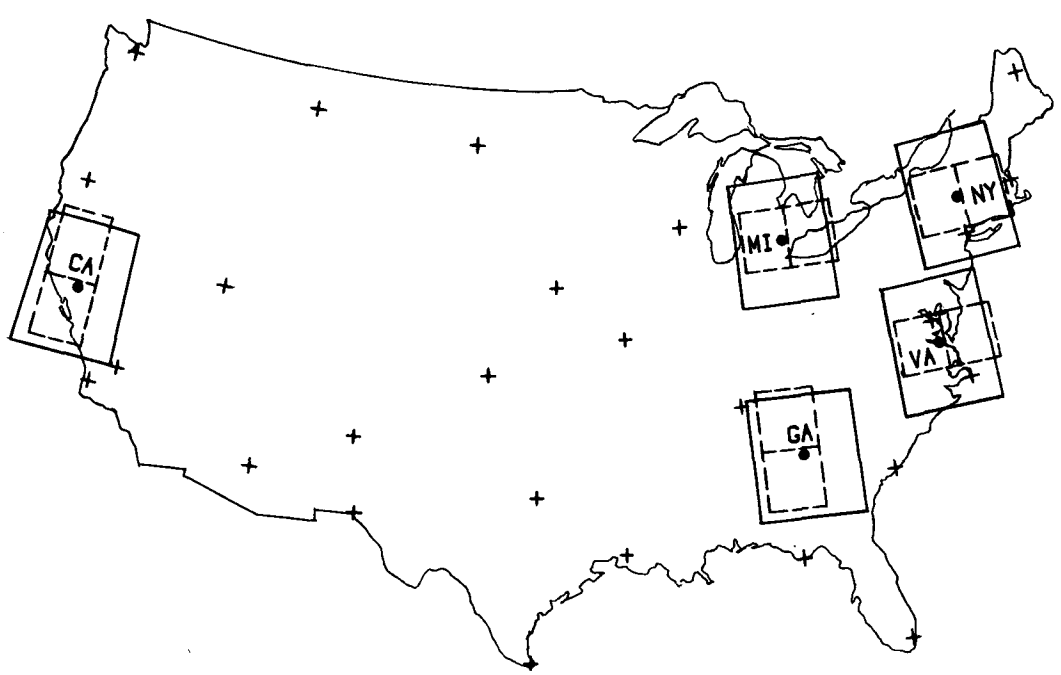

FIG. 1. Locations of five university sites (solid circles) and 26 SOLMET stations (crosses). Large rectangles are 5° × 5° TOVS data areas and dashed rectangles at each site are 2.5° × 2.5° HBP data regions.

pressure, total ozone burden, and channel radiances of each sensor. Surface pressure and elevation data are appended to the data stream from ephemeris information. For this technique, only TOVS total precipitable water vapor and ozone burden, selected HIRS-2 channel radiances, and surface pressure are required. A description of the TOVS instrument and TOVS data retrieval techniques is given by Smith et al. (1979).

For our validation analysis, only the TOVS boxes which fell within a 5° × 5° latitude–longitude area around the site were used (Fig. 1). An inverse-square-distance weighting procedure was applied to these data to give the greatest emphasis to data from the boxes closest to the ground site. A summary of the ranges of values of the meteorological parameters retrieved from the TOVS meteorological data at each site is given in Table 1.

The Heat Budget Products (HBP) retrieved from AVHRR measurements are produced daily on a global basis at 2.5° × 2.5° ground resolution. While several data products are available on the HBP tapes, only the top-of-the-atmosphere (TOA) albedo data were used to determine cloud transmittance, as discussed later. The AVHRR instrument and HBP data retrievals are described by Gruber (1978).

NOAA-6 satellite data were available over the entire 1-yr data period; however, data from the NOAA-7 satellite, with its more desirable daylight crossing time (1430 LST), were available only after mid-August 1981 (10.5 months), which resulted in a division of the present analyses into three time periods. First, because TOVS meteorological data from NOAA-6 alone (0730/1930 crossing times) were adequate for the clear-sky studies during the first 1.5 months, the clear-sky analysis extends over the entire 1-yr period. Second, HBP albedo data from NOAA-7 (1430 orbit crossings) were found to be necessary for daytime cloud modeling, and thus, the all-sky daily analyses covered only the last 10.5 months of the period. Third, since complete periods are required for monthly averages, the five-site results could be provided only for the last 10 months. Approximately a sixth of the days were not analyzed because of the absence of pyranometer, TOVS, or HBP data.

TABLE 1. Summary of satellite-derived meteorology.

Site	Water vapor range (pr cm)	Ozone range (atm cm)	Surface* pressure (mb)
CA	0.5–3.5	0.27–0.40	1011.1
GA	0.4–3.5	0.27–0.40	974.4
VA	0.4–2.9	0.28–0.41	1010.3
MI	0.2–2.6	0.31–0.46	978.5
NY	0.2–2.3	0.31–0.43	1003.7

* Nominal surface pressure based on site elevation.

3. Insolation model

The insolation model uses a broadband shortwave approach which assumes that instantaneous insolation at the surface, I_S, can be estimated from the product of insolation at the top of the atmosphere, I_{TOA}, clear-sky atmospheric transmittance, T_A, and cloud transmittance, T_C,

$$I_S = I_{TOA} T_A T_C. \quad (1)$$

In this study, first a model for T_A was developed for clear-sky conditions using TOVS meteorological data, and then a model for T_C was developed for all-sky conditions using HBP albedo data.

a. Clear-sky model

For clear-sky conditions ($T_C = 1$), Eq. (1) can be approximated as

$$I_S = S \cos\theta e^{-D_\theta} \quad (2)$$

where S is the Earth–Sun distance-corrected solar flux, θ is the solar zenith angle, and D_θ is the broadband atmospheric optical depth. Inspection of the 1-yr ground datasets showed that out of a total of 1609 days represented by the five sites, only 160 days were totally cloud free from sunrise to sunset and had complete ground and satellite data. For investigative purposes, hourly values of D_θ were computed for these days from site pyranometer measurements (I_S) as

$$D_\theta = -\ln[(\overline{I_S}\ \overline{\sec\theta})/S] \quad (3)$$

where $\overline{I_S}$ and $\overline{\sec\theta}$ are hourly integrated values. Plots of $\log D_\theta$ versus $\log \sec\theta$ are illustrated in Fig. 2.

We found that "clear-sky" conditions required that the day be not only cloud-free, but also have high surface visibility, and be free of haze, fog, smoke, etc. Reasons for this stringent requirement are discussed later. The required clear-sky conditions were found to exist when the linear correlation coefficient of each daily dataset, similar to those given in Fig. 2, was ≥ 0.97. Only 54 of the 160 clear-sky days met this pristine clear-sky requirement. For example, only the bottom five data plots of Fig. 2 (one shown for each site) met the requirement; the top two did not due to clouds or hazy conditions during part of the day.

Based on the approximately linear relation of $\log D_\theta$ and $\log \sec\theta$ for clear-sky conditions, the relationship between D_θ and $\sec\theta$ can also be expressed as

$$D_\theta = D_0(\sec\theta)^N \quad (4)$$

where D_0 is determined from the line intercept and N is the line slope. Physically, D_0 can be taken as the clear-sky, vertical optical depth for overhead Sun conditions, while $(\sec\theta)^N$ is an angular power function accounting for the change of optical depth with solar zenith angle. In Eq. 4, D_0 is the resultant optical depth arising from all absorption and scattering processes

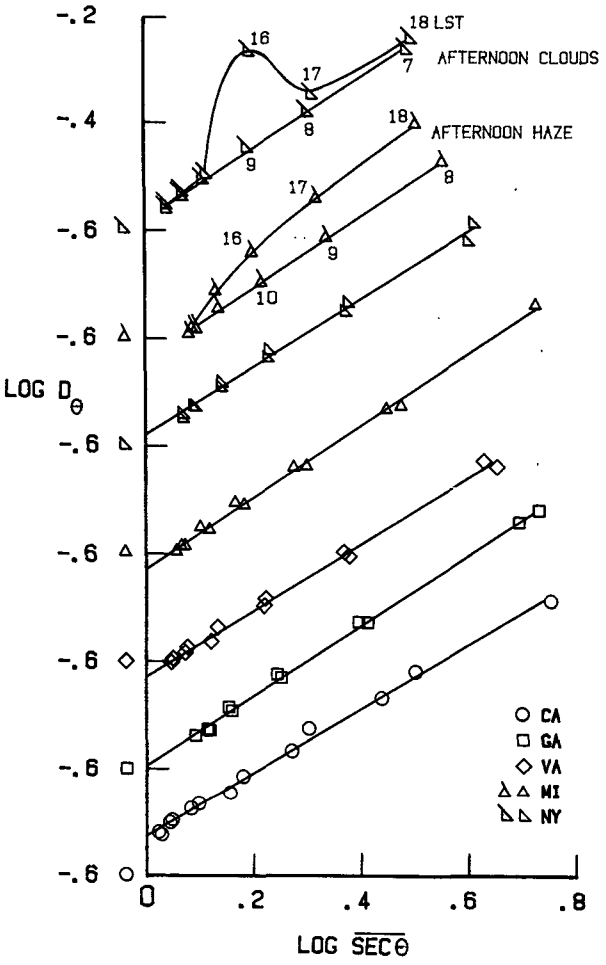

FIG. 2. Relationship of hourly values of D_θ and sec θ (Eq. 2). Note stepped vertical scales.

acting on the vertical radiation. Individual, well-developed vertical optical depth models are available to represent most of these atmospheric scattering and absorption processes. The optical depths of these separate components are generally either small or spectrally nonoverlapping; therefore, D_0 can be represented for the most part by the sum of these individual optical depths as

$$D_0 = D_{H_2O} + D_{O_3} + D_{O_2} + D_{CO_2} + D_{Ray} + D_{Alb} + D_{Aeros}. \quad (5)$$

The first four components represent solar radiation absorption due to atmospheric water vapor, ozone, oxygen, and carbon dioxide, respectively. They can be expressed individually as

$$D_{H_2O} = 0.104(U_{H_2O})^{0.30}, \quad (6)$$

$$D_{O_3} = 0.038(U_{O_3})^{0.44}, \quad (7)$$

$$D_{O_2} = 0.0075(P)^{0.87}, \quad (8)$$

and

$$D_{CO_2} = 0.0076(P)^{0.29}, \quad (9)$$

where U_{H_2O} is satellite-derived precipitable water vapor burden (pr-cm), U_{O_3} is satellite-derived ozone burden (atm-cm), and P is nominal surface air pressure (atmospheres). Equations (6) and (7) are approximations provided by Lacis and Hansen (1974), and Eqs. (8) and (9) are from Yamamoto (1962).

The Rayleigh scattering component is given by

$$D_{Ray} = 0.038P, \quad (10)$$

where 0.038 is the value derived by Lacis and Hansen (1974). The D_{Alb} term represents atmospheric backscattering of the surface-reflected flux, and has been approximated as

$$D_{Alb} = -0.065PA_S, \quad (11)$$

where A_S is the surface albedo and the coefficient 0.065 is the average of values given by Lacis and Hansen (1974) and Hoyt (1978). A value of $A_S = 0.14$ for no snow conditions and $A_S = 0.66$ for snow conditions was used for the present sites based on work by Kondrat'ev (1972).

The one remaining component of Eq. (5) to be considered is the aerosol scattering component, D_{Aeros}. Unlike the previous six components given by Eqs. (6) through (11), satellite measurements are not available from which to compute D_{Aeros}. Therefore, D_{Aeros} was determined empirically by a residual technique as follows. First, total vertical optical depths (D_0) for the 54 pristine clear-sky days were computed using Eqs. 3 and 4. These data are shown in Fig. 3 (top) plotted as a function of TOVS water vapor burden, U_{H_2O}. For these same days, satellite data were then used to compute the optical depths for the other six components (Eqs. 6–11). The residual optical depth of each day was attributed to D_{Aeros}, and these values of D_{Aeros} are presented in Fig. 3 (bottom), also as a function of water vapor burden. Fenn et al. (1981) found that lower tropospheric aerosols and relative humidity were correlated, and while the present correlation is not strong, D_{Aeros} does appear to increase with increasing U_{H_2O}. Therefore, in the present study, D_{Aeros} was represented as

$$D_{Aeros} = D_{Aeros,0} + 0.013U_{H_2O} \quad (12)$$

where $D_{Aeros,0}$ is the intercept value when $U_{H_2O} = 0$. Here $D_{Aeros,0}$ ranged from 0.01 to 0.05 (Fig. 3, dashed lines) and is probably influenced by the degree of the pristine condition of the atmosphere, the random error in U_{H_2O}, and the water content of the surface-level aerosols. The nominal value of $D_{Aeros,0}$ for our five-site analysis was 0.03 (Fig. 3, solid line), and it is believed this value could be used for most conditions (see sensitivity analysis later). It should be recognized that since D_{Aeros} is derived through a residual technique, it will

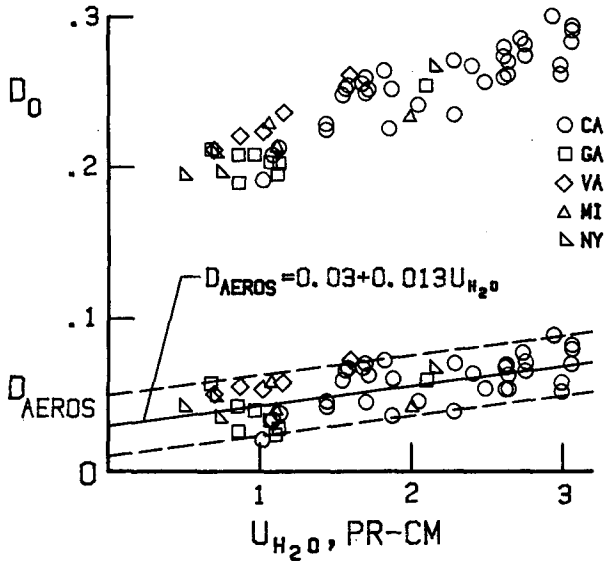

FIG. 3. Variation of the total optical depth (D_0) and aerosol optical depth (D_{Aeros}) with water vapor burden (U_{H_2O}) for clear-sky conditions.

also include any other unaccounted for atmospheric effects and errors in the overall clear-sky transmission. Except in very dry desert climates with long periods of blowing dust, these errors are expected to be quite acceptable.

With the TOVS input model for D_0 now complete, the only term needed to compute D_θ from Eq. (4) is N. Values of N were determined from the slopes of $\log D_\theta$ versus $\log \sec\theta$ plots for the 54 clear-sky days and are presented in Fig. 4 as a function of D_0, the parameter for which the best correlation was obtained. Regression analysis of the data shows the relationship of N and D_0 to be

$$N = 1.1 - 2.0D_0 \tag{13}$$

and while the correlation for this equation is not high, it has a degree of validity in radiative transfer. That is, for weak absorbers (i.e., D_0 small), optical depth (D_θ) is nearly linear ($N \approx 1$) with absorption path ($\sec\theta$), while for strong absorbers (i.e., large D_0), D_θ is less than linear ($N \leq 1$) with $\sec\theta$.

The clear-sky optical depth can now be expressed as

$$D_\theta = D_0(\sec\theta)^{1.1-2.0D_0} \tag{14}$$

and totally evaluated using only TOVS satellite-determined parameters. Figure 5 shows a comparison of the 740 satellite-estimated and ground-measured hourly insolation values for the 54 clear-sky days. These same values, summed daily and divided by 24 (to be consistent with the majority of radiation budget studies), are compared in Fig. 6.

b. *All-sky model*

For all-sky conditions the cloud transmittance factor, T_C, must be determined. Clouds are the most prominent factor affecting surface insolation over most regions of the globe and must be characterized radiatively before accurate estimates of surface insolation can be made for all-sky conditions.

One of the original goals of the present study was to characterize cloud effects on insolation using only TOVS data. The TOVS algorithm for retrieving cloud data relies mainly on infrared channel data, and frequently does not detect lower level clouds or fog when higher level clouds exist in the same box. Thus, the TOVS cloud data were found to be inadequate for surface insolation estimation. In the present technique, all-sky TOA albedo data are used, as derived from operational NOAA heat budget products (HBP) data. Heat budget products TOA albedo data are generated from the AVHRR visible channel (0.57–0.69 μm) radiances obtained from the NOAA-7 satellite. The HBP data, which are based on 2.5° × 2.5° surface areas over the globe, have centers that do not coincide with any of the five university sites (see Fig. 1). Therefore, the TOA albedo values from the two areas nearest each site were simply averaged to obtain the site albedos.

The development of the cloud transmittance model began with a computational approach. Cloud transmittances were computed as the ratio of ground-measured insolations (all-sky conditions) to satellite-estimated clear sky insolation values from the five university sites. The effective daily cloud transmittance was computed as

$$T_C = I_{S,M}/I_{S,CS} \tag{15}$$

where $I_{S,M}$ is the daily total ground-measured insolation and $I_{S,CS}$ is the daily total satellite-estimated, clear-sky

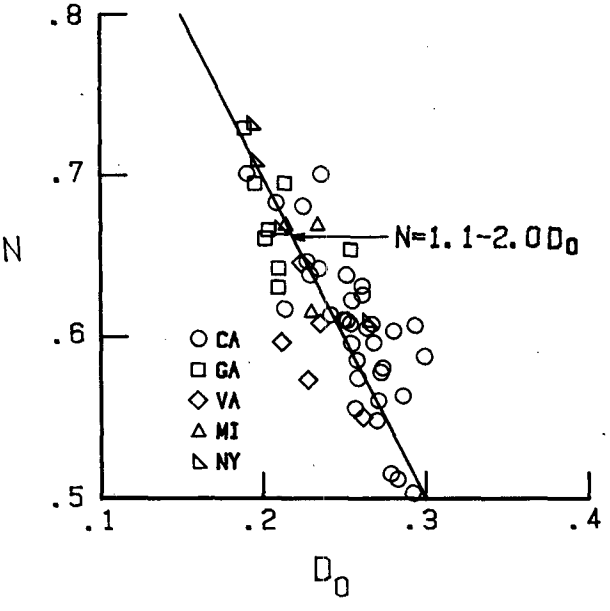

FIG. 4. Relationship of the exponent N with total optical depth (D_0) for clear-sky conditions.

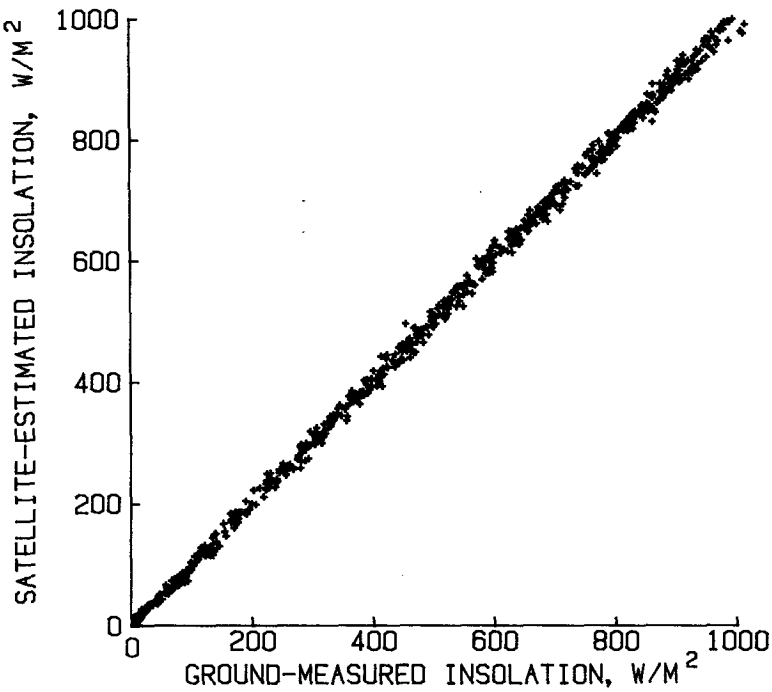

FIG. 5. Comparison of estimated and measured hourly insolation for clear-sky conditions.

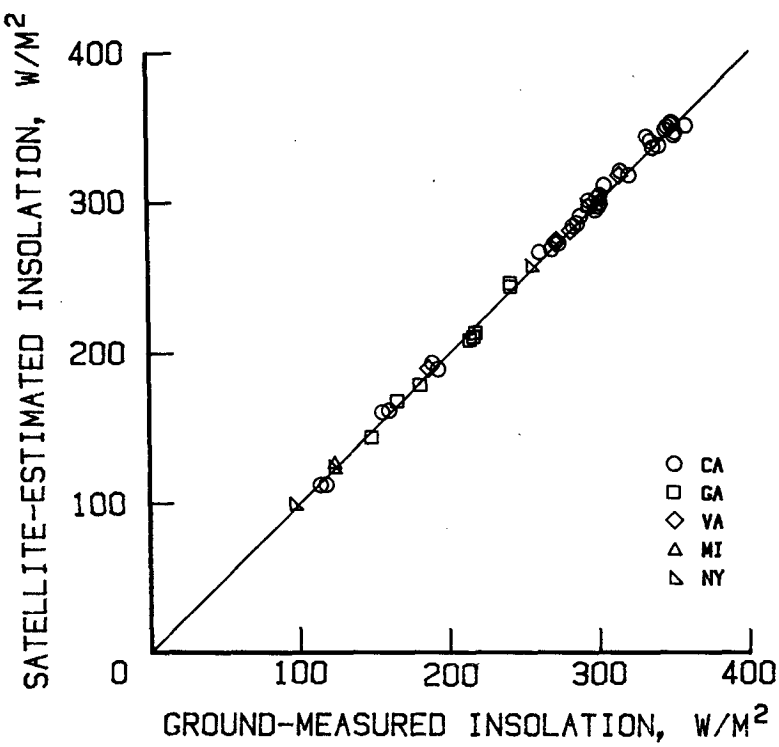

FIG. 6. Comparison of estimated and measured daily average insolation for clear-sky conditions.

insolation, both summed for daylight hours in each day. A comparison between these computed effective daily cloud transmittances, T_C, from all sites for the full year (1329 days) and the measured daily TOA albedos was made. A strong relationship between the daily T_C value at each site and the daily satellite TOA albedo value at each site could be established. As an example, the computed cloud transmittances, T_C, for the NY site are plotted as a function of the daily TOA albedos in Fig. 7(a) for 157 days during which there

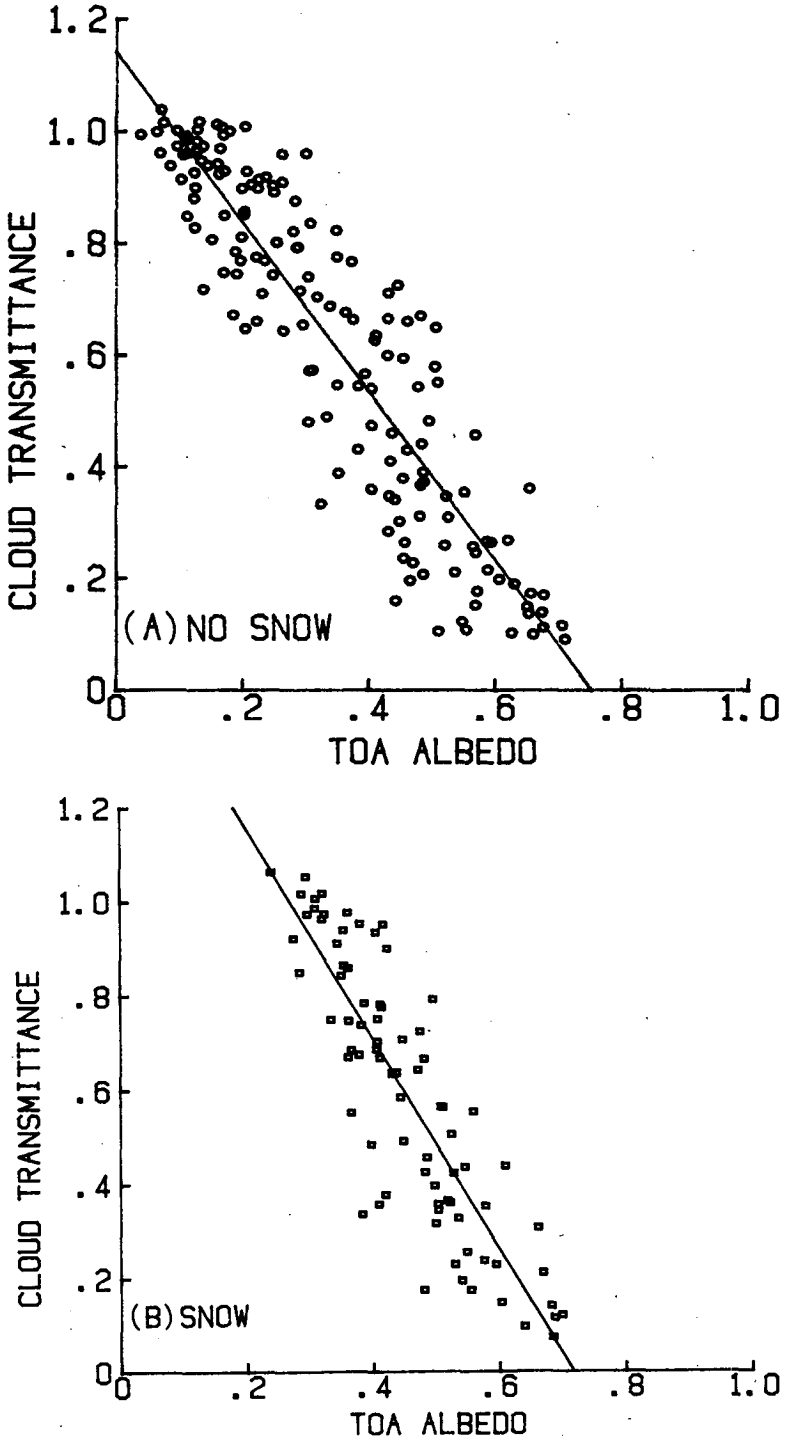

FIG. 7. Relationship between daily cloud transmittance and TOA albedo for NY site: (a) no snow cover, (b) snow cover.

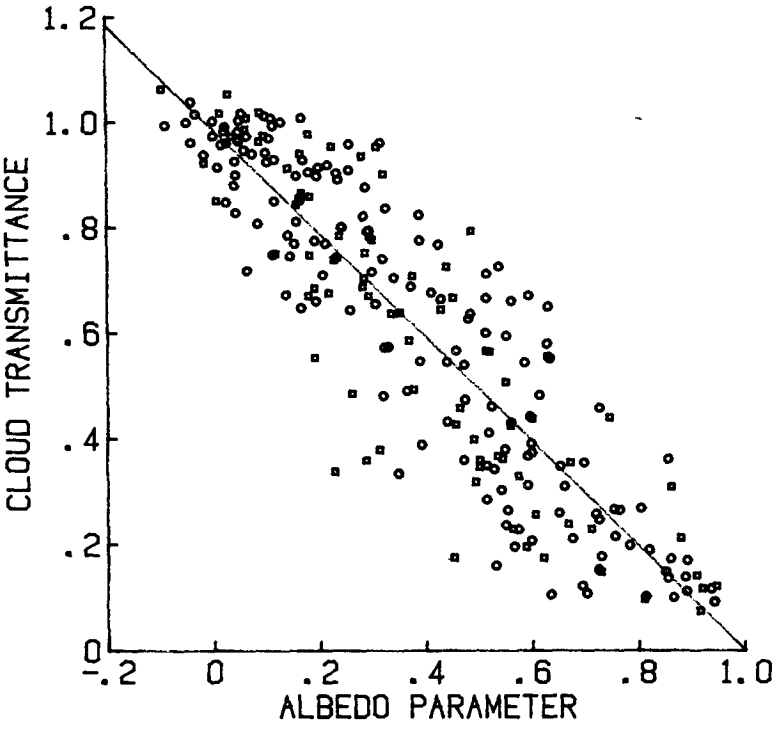

FIG. 8. Relationship between daily cloud transmittance from NY ground-measured data and computed albedo parameter. Circles represent no-snow days; squares, snow-covered days.

was either no snow or less than an inch of snow on the ground. In Fig. 7(b) similar data are plotted for the 80 days during which there was 1 in. or more of snow. While there is considerable scatter, the data in each of the plots can be reasonably represented by a straight line.

As a result of the linear relationship demonstrated between computed values of T_C and the TOA albedo at the university sites for all seasonal conditions, the daily effective cloud transmittance for the general case could also be expressed as

$$\hat{T}_C = 1 - A_p \tag{16}$$

where $\hat{T}_C$ is an *estimated* effective daily cloud transmittance and A_p is a normalized albedo parameter defined as

$$A_p = (A - A_1)/(A_0 - A_1) \tag{17}$$

where A is the area-averaged TOA albedo value from the HBP data, and A_1 and A_0 are regression-determined values of TOA albedo for the limiting conditions of $\hat{T}_C = 1$ and 0 (totally clear, totally overcast), respectively. The $\hat{T}_C$ values for the NY site are presented in Fig. 8 as a function of the albedo parameter for the combined 237 snow and no-snow days. The regression-determined values of A_1 and A_0 for all five sites are given in Table 2. There was no snowfall at the CA site and no substantial snowfall at either the GA or VA sites during the 1-yr data period.

Using the described T_C technique, surface insolation can now be estimated for all-sky conditions using Eq. (1) where T_A is evaluated from TOVS meteorological data and $\hat{T}_C$ is evaluated from HBP TOA albedo data. A comparison between the 1329 satellite-estimated daily insolation fluxes and ground-measured fluxes at the five sites is shown in Fig. 9. Measured and estimated monthly insolation fluxes for each site, determined from the averages of the available daily fluxes during the last 10 months of the data period (September 1981 through June 1982), are compared in Fig. 10. A sum-

TABLE 2. Summary of albedo constants by regression method.

Site	Days*	A_1	A_0	$A_{0.1}$
CA	255	0.078	0.738	0.672
GA	281	0.085	0.756	0.689
VA	284	0.079	0.763	0.695
MI (no snow)	194	0.104	0.738	0.675
(snow)	78	0.394	0.715	0.683
NY (no snow)	157	0.097	0.747	0.682
(snow)	80	0.282	0.722	0.678
Total	1329			

* Number of days for which ground insolation, TOVS and HBP data were *all* available.

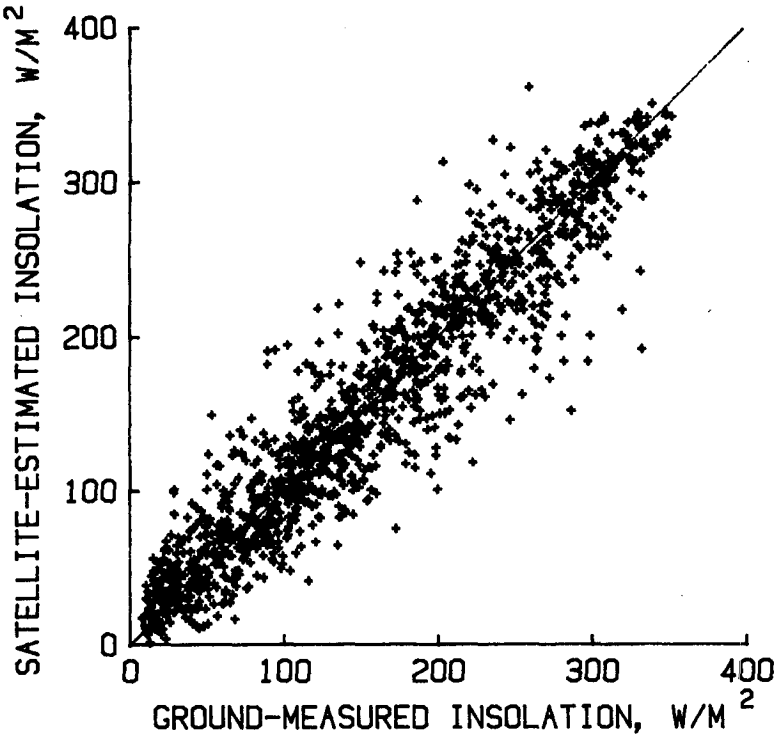

FIG. 9. Comparison of estimated and measured daily average insolation from the five university sites for all-sky conditions.

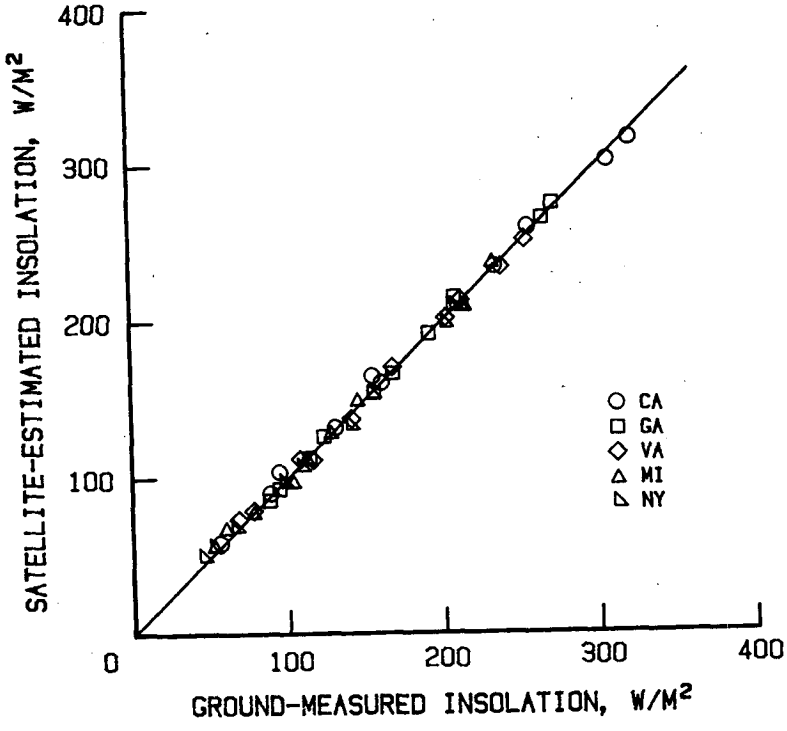

FIG. 10. Comparison of estimated and measured monthly average insolation for all-sky conditions.

mary of the estimation statistics on an hourly, daily, and monthly basis is given in Table 3.

The regression technique for determining A_1 and A_0 was utilized for the five university sites because ground data existed. In general, however, these data will not be available, and an alternate technique is proposed that does not depend on regression data. The alternate technique evaluates A_1 and A_0 through the use of histograms of the measured daily TOA albedo taken over any region of interest. Figure 11 illustrates such a histogram for the NY site. Different curves are shown for no-snow and snow-covered surface conditions since these conditions must be treated individually. These data were constructed from a 1-yr HBP TOA albedo data set (1 September 1981 to 31 August 1982) taken by NOAA-7. The vertical lines near the left end of each curve indicate the A_1 values which were defined by the regression approach to best represent the clear-sky TOA albedo condition (ie., $T_C = 1$). These values for A_1 might have been expected to occur at the extreme minimum albedo value on the curves. Notice that instead, the A_1 lines lie about 0.03 above the extreme minimum albedo value for each curve. This small increase is a practical adjustment of the A_1 value to allow for the known cyclic variations of the TOA albedo which are discussed in the next section. Therefore, in the histogram technique $A_1 = A_1' + 0.03$, where A_1' is the minimal value on the histogram curve.

At the extreme right end of the Fig. 11 curves, the maximum albedo value represents A_0; however, as with the A_1 determination, a practical adjustment must be made. Note in Figs. 7(a) or (b) that in the practical case, T_C never drops to a value of 0 and a practical minimum T_C occurs at about 0.1. Thus, a TOA albedo value must be determined on the histogram curve that represents the condition of $T_C = 0.1$. Given the values for A_1 and A_0, the albedo corresponding to the $T_C = 0.1$ condition can be computed as

$$A_{0.1} = 0.9A_0 + 0.1A_1. \quad (18)$$

On the histogram, this condition is represented by the vertical lines labeled $A_{0.1}$. Both the no-snow and snow cases have essentially the same $A_{0.1}$ values indicating, as it should, that TOA albedo is independent of surface albedo under totally overcast conditions. The regression values of A_1 and A_0 can also be used to determine values for $A_{0.1}$. The $A_{0.1}$ values determined from the regressions for each university site are listed in Table 2. The range of $A_{0.1}$ values is quite small, suggesting that 0.68 may be a reasonable global constant for $A_{0.1}$. Some verification of the computed value of $A_{0.1}$ can be found

TABLE 3. Summary of insolation estimation statistics.

Parameter	Clear-sky Hourly	Clear-sky Daily	All-sky Daily	All-sky Monthly
All-site data				
Data period (months)	12.0	12.0	10.5	10.0
No. of computed fluxes	740	54	1329	50
Average flux (W m^{-2})	461.96†	263.77	157.38	154.56
Standard error (W m^{-2})	10.59	4.42	30.22	4.21
Std. error rel. to av flux (%)	2.3	1.7	19.2	2.7

	Site CA	GA	VA	MI*	NY*
Single-site data (all-sky daily average)					
Data period (months)	10.5	10.5	10.5	10.5	10.5
No. of computed fluxes	255	281	284	272	237
Averge flux (W m^{-2})	179.5	171.5	164.6	138.8	130.2
Standard error (W m^{-2})	21.82	34.76	32.42	32.63	26.95
Std. error rel. to av flux (%)	12.2	20.3	19.7	23.5	20.7
Single-site data (all-sky, monthly average)					
Data period (months)	10	10	10	10	10
No. of computed fluxes	10	10	10	10	10
Average flux (W m^{-2})	181.1	168.2	159.3	134.7	129.4
Standard error (W m^{-2})	5.02	4.03	4.35	4.97	4.61
Std. error rel. to av flux (%)	2.8	2.4	2.7	3.7	3.6

† Daylight hours.
* No-snow and snow-covered results combined.

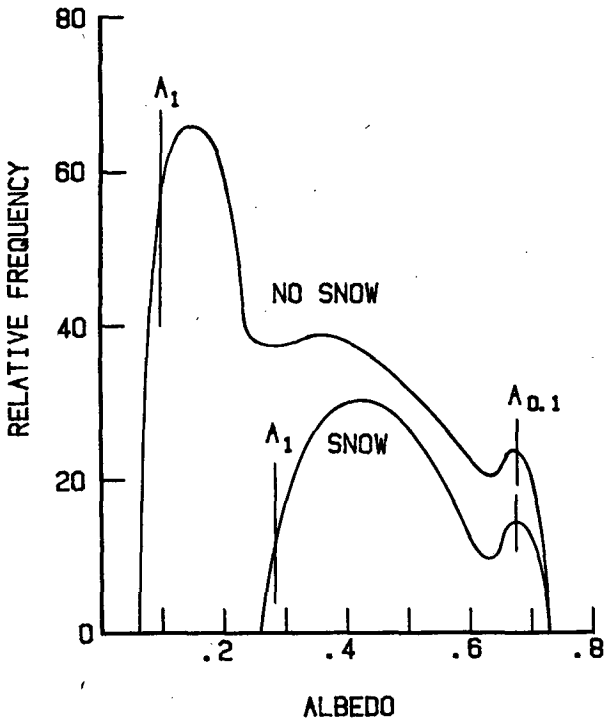

FIG. 11. Histograms of TOA albedo values from NOAA-7 for NY site during 1-yr period (September 1981 through August 1982), for no-snow and snow-cover conditions. Vertical lines indicate the albedo constants determined by the regression technique (Table 2).

in the fact that the $A_{0.1}$ value of Fig. 8 coincides with the frequency peaks near the right side of Fig. 11.

4. Error analysis

An error analysis was conducted to establish the sensitivity of the daily flux results to errors in the input data. Sensitivities, listed in Table 4, were computed by perturbing each input parameter about its nominal value by an amount equal to the expected measurement error. Flux error sensitivities are also a function of site latitude and solar declination, and hence, for these analyses, a latitude of 40° and a solar declination of 0° was used as part of the nominal condition. Discussion of the clear-sky and all-sky flux error sources follows.

a. Clear-sky

The clear-sky flux errors shown in Table 4, produced as a result of TOVS errors, are relatively small. The listed errors are consistent with the 1.7% daily clear-sky error result given in Table 3.

b. All-sky

All-sky flux errors are relatively large. The TOA albedo, A_1 and A_0, and snow detection are the three prime contributors to all-sky errors and will be discussed individually.

Errors in the determination of TOA albedo can produce the largest errors in the daily all-sky insolation results. A perturbation of ±0.08 was assigned to TOA albedo (A) in Table 4, and the resultant flux error was ±20%, consistent with the 19.2% daily flux error given in Table 3. The TOA albedo determination necessarily involves several assumptions, and these will be discussed in detail.

Part of the TOA albedo error is caused by AVHRR radiometer measurement error. This measurement error is believed to be random in nature and quite small, especially on a monthly basis. Another contribution to TOA error is from angular viewing errors. The TOA albedo values derived from HBP data are actually narrowband TOA bidirectional reflectances applicable at the moment the satellite sampled the subsatellite area. Conversion of these reflectances to albedo values requires knowledge of the instantaneous solar zenith, viewing zenith, and viewing azimuth angles. These angles are not given on the HBP tapes, and hence, we have assumed the surfaces to be Lambertian. The NOAA-7 satellite had a 9-day groundtrack repeat cycle, where ground sites were viewed for the first 3 days at

TABLE 4. Insolation errors (based on daily values)†.

Nominal value	Perturbed value	Insolation error, %
	Clear-sky	
U_{H_2O} = 1.6 pr-cm	1.8	−0.7
	1.4	+0.8
U_{O_3} = 0.35 atm-cm	0.40	−0.2
	0.30	+0.2
P = 1000 mb	1020	−0.1
	980	+0.1
A_S = 0.14	0.16	+0.2
	0.12	−0.2
$D_{Aeros,0}$ = 0.03	0.04	−1.2
	0.02	+1.2
	All-sky	
A = 0.35	0.43	−20.0
	0.27	+20.0
A_1 = 0.10	0.12	+3.2
	0.08	−3.0
A_0 = 0.75	0.78	+2.8
	0.72	−3.0
	Unidentified snow	
A = 0.35*	0.35*	
A_1 = 0.10	0.35	
A_0 = 0.75	0.72	+68.8
A_S = 0.14	0.66	

† At 40° latitude and solar declination of 0°.
* No error.

large viewing zenith angles from the east, then for 3 days at small viewing zenith angles from the nadir, and lastly for 3 days at large viewing zenith angles from the west. The effect of the 9-day cycle on the "albedo" is illustrated in Fig. 12 for two relatively cloud-free cases, the Libyan desert (top curve) and the Arabian Sea (bottom curve), during October 1981. (None of the five university sites had a sufficient number of consecutive cloud-free days to properly illustrate this effect.) Approximately ±0.04 daily albedo variability occurs about the monthly average values of the curves of Fig. 12 (dashed lines). This variability produces daily flux errors of about ±10%; however, on a monthly basis the 9-day cycle effect is mostly averaged out. This cycle-averaging is believed to be the major reason that the monthly average insolation error was reduced to only 2.7%. Compared to the daily average error of 19.2%, this represents a decrease by a factor of 7, while a factor of only about 5 would be expected due to monthly averaging, assuming normal, uncorrelated errors. Although the HBP data are narrow-band (0.57–0.69 μm) albedos, this should cause little, if any, error due to the fact that the A_1 and A_0 values used to estimate T_C (Eqs. 16 and 17) are also derived from the same narrow-band data.

At the present time, the histogram technique for determining A_1 and A_0 has not been demonstrated for all global conditions. It is believed, however, that the technique will permit accuracies of ±0.02 and ±0.03 for A_1 and A_0, respectively, as given in Table 3.

The disparity of views between the satellite and the pyranometer is another source of error. In our TOA albedo calculation, it has been assumed that the same cloud scene was being viewed by the down-looking satellite as by the up-looking ground-based pyranometer. This assumption is applied in the regression relation developed between TOA albedo and cloud transmittance where cloud transmittance is determined from the surface readings of the pyranometer. However, the surface area of the two 2.5° × 2.5° regions from which the averaged HBP albedos were obtained is about 10^5 km^2, while a ground-site pyranometer has an effective areal coverage of about 10^3 km^2. This large discrepancy in sampling coverage could produce large errors for worst-case conditions. For instance, the skies over a pyranometer could be totally overcast, while the effective cloudiness for the region might be only a few percent. This spatial error occurs, however, only when the present technique is applied to small areas such as pyranometer sites, and is not applicable when the technique is applied to large regions (10^6 km^2) as planned.

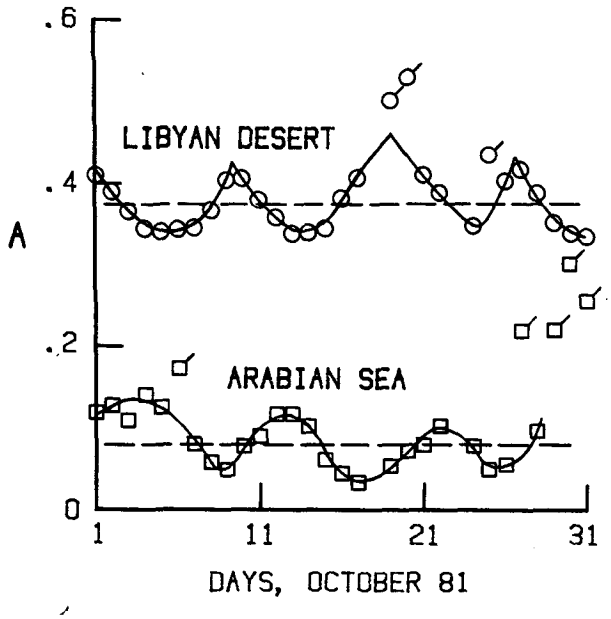

FIG. 12. Illustration of the 9-day cyclic variation of TOA albedo from NOAA-7. Flagged symbols denote cloudy conditions. Horizontal dashed lines represent averaged clear-sky albedos for the month.

The final source of error in the TOA albedo model stems from the use of one instantaneous satellite sampling to characterize the daily cloud condition. The NOAA-7 satellite provides only one albedo measurement per day, based on the 1430 LST equatorial-overpass orbit. This orbit provides nominally one daylight overpass of all regions, except during winter in the extreme polar cap regions when darkness prevails. Once-per-day sampling can, in some areas, result in large TOA albedo errors, and thus may be the major source of error in the all-sky insolation technique. For instance, the skies could be mostly cloudy at overpass time, while mostly clear on a daily basis. Generally, the 1430 LST orbit is thought to provide a good daily sampling time, but may present problems in the tropics where large diurnal variations can be expected. This problem is inherent in all techniques based on sun-synchronous satellite data and, indeed, is the penalty to be paid to achieve total global coverage. Improved temporal sampling of clouds will soon be possible by utilizing the database of the International Satellite Cloud Climatology Project (ISCCP), which will provide meteorological parameters every 3 hours. These data will be incorporated in the proposed technique as soon as available, which will also eliminate the spatial discrepancy problem discussed previously.

By far the largest error of those listed in Table 4 can be caused by not recognizing the presence of snow cover and not adjusting A_1 and A_0 accordingly. That is, if a surface area was assumed to be snow-free but was actually snow-covered, or vice versa, a large flux error would result. This problem will exist for only a very small portion of the globe, and over much of this, only during limited times of the year. These areas are where accurate surface radiation data will be very important to climate studies. An acceptable operational technique must provide continuous determination of the surface snow-cover condition over all regions of the globe.

Clouds and snow are usually both bright and cold

making it difficult for visible and thermal radiometers to differentiate them. At 4-μm wavelengths, however, clouds remain bright while snow and ice appear dark. Weekly averaged reflectance ratios of HIRS-2 channels 18 (4 μm) and 20 (0.7 μm) for the NY site are presented in Fig. 13. The Earth-emitted radiation component of channel 18 was removed using the blackbody temperature values from channel 8 (11 μm). Further, the reflectance ratios were normalized by the average of the values obtained during the first 5 weeks of the period when no-snow conditions prevailed.

The reflectance ratio (Fig. 13) dropped to a lower value with the first snowfall in early December 1981 and remained there until the snow began to melt in early March 1982. As the snow melted, the reflectance ratio increased, but returned briefly to a lower value in early April when a 13-in. snowfall occurred on 5–6 April 1982. The required inputs are part of the TOVS data, and it is believed the reflectance ratio technique will be adequate to detect the presence of snow on a regional basis over the globe.

5. Results and discussion

a. Clear-sky conditions

The ability of the clear-sky insolation model to accurately estimate fluxes was tested by using only 54 pristine clear-sky days out of the total of 160 cloud-free days at the five university sites. This approach was necessary because haze, fog, smoke, etc. that occurred during the remaining 106 nonpristine days were found to have increased their TOA albedo values 0.027, on the average, over those of the pristine days. In effect, near-surface turbidity on these 106 days was being sensed in the TOA albedos as a small amount of cloudiness. Use of only the 54 pristine clear-sky days provided comparisons between 740 hourly satellite-estimated and ground-measured flux pairs during the 1-yr data period. The largest number of comparisons came from the CA site where the fairest weather prevailed. Figure 5 shows the hourly results from all sites. The bias between the satellite-estimated and surface-measured fluxes was less than 0.42%, and the measurement error was 11 W m^{-2}, which was 2.34% of the average ground-flux value. Daily average insolation results for these 54 pristine clear-sky days are shown in Fig. 6. The measurement error was 4 W m^{-2} or about 1.7% of the average measured flux which was 264 W m^{-2}.

b. Clear-sky, nonpristine conditions

The 106 clear-sky days which had moderate amounts of turbidity were considered as a separate class. Even this amount of turbidity produced slightly higher TOA albedos, as stated above, and the average estimated $\hat{T}_C$ value (using Eqs. 16, 17) for these days was 0.958 rather than approximately 1 for a pristine clear-sky case. Considering that the overall computed value of T_C from the ratio of the daily surface-measured to satellite-estimated clear-sky insolation averaged 0.964 (using Eq. 15), the effect of turbidity on the clear-sky, nonpristine days was remarkably well accounted for by the all-sky technique.

c. Clear-sky model validation

As a general rule, it is desirable to validate an insolation model using datasets that are independent from those involved in the derivation of the model itself (i.e., dependent vs independent). The independent site data used here for validation consisted of an insolation dataset compiled by NOAA from 26 SOLMET stations which, when combined, represented 544 station-years of measurements (SOLMET 1979). Locations of the 26 stations are tabulated in Table 5 and shown in Fig. 1 (crosses) where they are seen to be broadly distributed across the United States. In SOLMET (1979), hourly clear-sky (not necessarily pristine) insolation values from these sites were regressed as a function of solar zenith angle in the form

$$I_S = a_0 + a_1 \cos\theta + a_2 \cos^2\theta + a_3 \cos^3\theta. \quad (19)$$

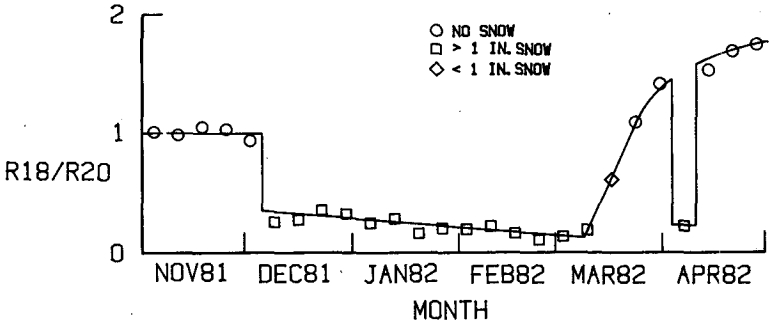

FIG. 13. Weekly averaged reflectance ratio for the NY site, illustrating the snow detection capability. Normalized to value of 1 for no-snow conditions in the first 5 weeks.

TABLE 5. Twenty-six station, clear-sky independent dataset.

Station	Years	Standard error (%)	Turbidity correction factor
Albuquerque (NM)	24	3.3	1.010
Appalachicola (FL)	24	7.9	1.056
Bismark (ND)	24	3.9	1.016
Boston (MA)	17	8.2	1.059
Brownsville (TX)	24	5.2	1.029
Cape Hatteras (NC)	24	4.7	1.024
Carribou (ME)	24	5.1	1.028
Charleston (SC)	24	5.4	1.031
Columbia (MO)	24	5.5	1.032
Dodge City (KS)	24	4.3	1.020
El Paso (TX)	24	3.4	1.011
Eley (NV)	14	3.5	1.012
Fort Worth (TX)	24	5.3	1.030
Fresno (CA)	16	4.3	1.020
Great Falls (MT)	16	4.1	1.018
Lake Charles (LA)	24	5.1	1.028
Madison (WI)	21	6.3	1.040
Medford (OR)	16	3.0	1.007
Miami (FL)	23	5.0	1.027
Nashville (TN)	24	6.4	1.041
New York (NY)	18	11.2	1.089
Omaha (NE)	19	4.4	1.021
Phoenix (AZ)	16	3.2	1.009
Santa Monica (CA)	17	4.0	1.017
Seattle–Tocoma (WA)	15	3.8	1.015
Washington (DC)	24	6.9	1.046
Total	544	Av 5.1	Av 1.028

For each of the 26 stations, monthly values of a_0, a_1, a_2 and a_3, as well as A_S and U_{H_2O}, were given in tabular form. This 26-station tabular dataset was used as the independent insolation data base with which our model could be tested and validated. Based on these values, the midmonth, noontime clear-sky insolations for the 26 stations were computed, using both the SOLMET regression equation and the present model. The results from the two approaches are compared in Fig. 14(a). Data points have been represented by one of three symbols depending on the percent standard error of each station's regression fit, as given in Table 5 (SOLMET 1979, Table 7). A close inspection of Fig. 14(a) reveals that 1) the majority of the high standard-error data (diamonds) lie at the top of the sequence of points; 2) the low standard-error data (circles) lie at the bottom; 3) the midstandard-error data (squares) lie between; and 4) the low standard-error data were in good agreement with the present model (line). This result was to be expected considering that the present model was based on only pristine, clear-sky conditions while the SOLMET data were constrained only to cloud-free conditions. The standard errors for the SOLMET data (Table 5) ranged from 3.0% for the probable near-pristine conditions at Medford, Oregon, up to 11.2% for the more turbid conditions expected for New York City.

The standard error of the hourly data for the present five-site model was 2.3% (Table 3). Assuming this value as a threshold standard error representing pristine conditions, a turbidity correction factor, C_{Turb}, given by

$$C_{\text{Turb}} = 1 + \frac{\text{Standard Error} - 2.3}{100} \tag{20}$$

was multiplied by the SOLMET station insolation flux data. The turbidity-corrected SOLMET flux results were then plotted as before with the present model estimated results as shown in Fig. 14(b). There are several notable features in this plot. First, the individual station standard errors are no longer clustered according to high-, mid-, or low-error amounts. Second, the mean difference between SOLMET and present model fluxes was reduced from 2.8% to zero. Third, the standard error of the SOLMET flux data was reduced from 4.1% to 2.4%. Most importantly, the present model fluxes and the corrected SOLMET fluxes are now in good agreement. This comparison with the 26-station, 544 station-year SOLMET dataset clearly establishes the general applicability of the present clear-sky insolation model for a wide range of surface conditions.

d. All-sky conditions

Daily all-sky insolations were calculated for each of the five sites during a 10.5-month period. The same computational approach was used as with the clear-sky insolations except that the hourly satellite fluxes were summed for each day before being compared with the ground-observed data. A composite scatterplot of all sites is provided in Fig. 9. The measurement error for 1329 daily fluxes was 30.2 W m^{-2} which is 19.2% of the average ground flux value of 157.4 W m^{-2}. The bias between the average satellite-estimated and ground-measured insolation flux values was 0.16% for the full data period. Between sites, standard error of estimate for the daily results appears to be greatest for the GA site (33.5 W m^{-2}) and lowest for the CA site (21.6 W m^{-2}). In terms of percent error, however, the MI site has the highest error (22.9%) since the average daily flux value for the MI site is lower. This amount of site-to-site variance was not present in the clear-sky data and thus must be attributed mostly to error introduced by the cloud transmittance technique.

Monthly averaging of the daily insolation was also performed. Ten monthly averages were produced for each of the five sites (Fig. 10). Monthly averaging of the data appears to reduce the cloud transmittance variability considerably. Monthly errors for the five-site combined dataset are reduced to about 4.2 W m^{-2}, which is 2.72% of the monthly ground flux average of 154 W m^{-2}.

As with the clear-sky model, it would be desirable to validate the all-sky model with an independent dataset. SOLMET (1979) does include regressions and analyses of insolation data for cloudy-sky conditions. Unfortunately, HBP albedo data for the 1952–76 time period during which the SOLMET data were taken are not available, and hence a comparison was not possible.

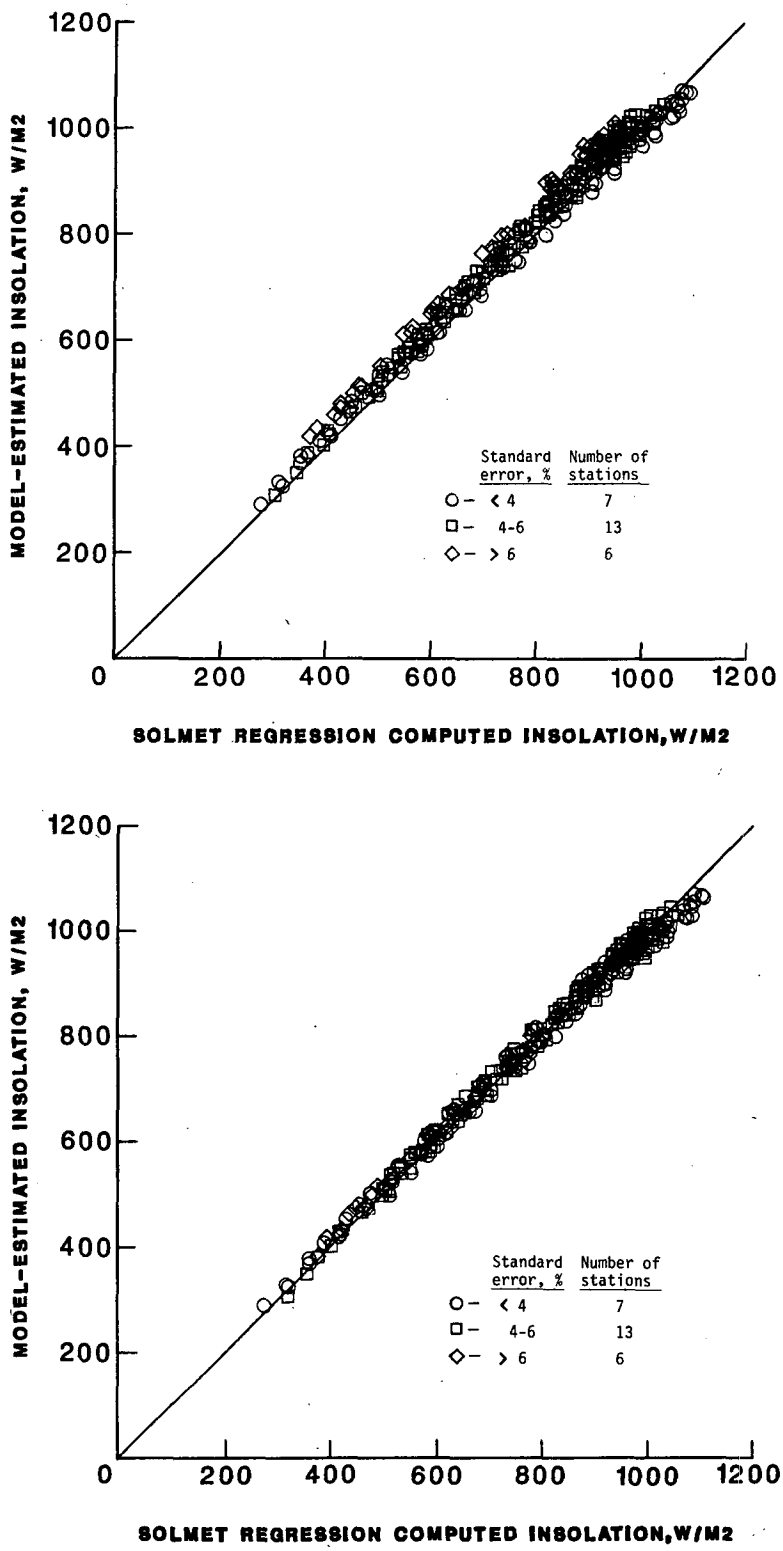

FIG. 14. Comparison of estimated and measured clear-sky, noon-time insolation for 26 SOLMET sites; (a) uncorrected for turbidy, mean error = 2.8%, standard error = 4.1%; (b) corrected for turbidity, mean error = 0%, standard error = 2.4%.

6. Conclusions

Daily and monthly insolation fluxes can be estimated using the proposed technique in combination with sun-synchronous satellite data. The required satellite data are TOVS and AVHRR operational data products. Validation of the technique was conducted using ground-truth data from five university sites and 26 SOLMET sites scattered throughout the United States and offering a wide variety of surface conditions. Accuracies achieved with this technique, based on the five university sites, were 19.2% for daily average values and 2.7% for monthly average values. The large reduction in the monthly errors was due, in part, to the canceling of spacecraft angular viewing errors for monthly results. The largest individual insolation errors which could occur with this technique are attributed to not recognizing snow cover. A method for detecting snow cover is included in the paper. Significant insolation errors could also occur if the once-per-day cloud cover readings by the satellite were nonrepresentative of the daylight period. On a monthly basis, it is believed that significant diurnal errors will not occur for most areas of the globe. Areas with large diurnal cloud variability, such as the tropics, may be the exception. Sensitivity studies were conducted for all the input parameters based on realistic perturbations about a nominal value for each parameter, and these results show the individual effects of measurement errors on the estimated insolation. Based on 1) the physical basis of the technique; 2) its validation at a variety of ground sites, and 3) its use of sun-synchronous satellite data, the technique is considered to be suitable for global estimations of insolation flux.

REFERENCES

Darnell, W. L., S. K. Gupta and W. F. Staylor, 1986: Downward longwave surface radiation from Sun-synchronous satellite data: Validation of methodology. *J. Climate Appl. Meteor.*, **25,** 1012–1021.

Diak, G. R., and C. Gautier, 1983: Improvements to a simple physical model for estimating insolation from GOES data. *J. Climate Appl. Meteor.*, **22,** 505–508.

——, C. Gautier and S. Masse, 1982: An operational system for mapping insolation from GOES satellite data. *Sol. Energy,* **28,** 371–376.

Ellis, J. S., and T. H. Vonder Haar, 1978: Solar radiation reaching the ground determined from meteorological satellite data. *Proc. Third Conf. on Atmospheric Radiation,* University of California, Davis, 187–189.

Fenn, R. W., E. P. Shettle, W. S. Hering and R. W. Johnson, 1981: Atmospheric optical properties and meteorological conditions. *Atmos. Environ.*, **15,** 1191–1918.

Gautier, C., G. Diak and S. Masse, 1980: A simple physical model to estimate incident solar radiation at the surface from GOES satellite data. *J. Appl. Meteor.*, **19,** 1005–1012.

Gruber, A., 1978: Determination of the Earth–atmosphere radiation budget studies. NOAA Tech. Rpt. NESS 76, 28 pp.

Hanson, K. J., 1971: Studies of cloud and satellite parameterization of solar irradiance at the Earth's surface. *Proc. Conf. on Remote Sensing,* Miami, Fla., U.S. Dept. Commerce, 133–148.

Hoyt, D. V., 1978: A model for the calculation of solar global insolation. *Sol. Energy,* **21,** 27–35.

Justus, C. G., M. V. Paris and J. D. Tarpley, 1986: Satellite-measured insolation in the United States, Mexico, and South America. *Remote Sens. Envir.*, **20,** 57–83.

Kondrat'ev, K. Ya., 1972: Radiation processes in the atmosphere. World Meteorological Organization Report WMO-309, 214 pp.

Lacis, A. A., and J. E. Hansen, 1974: A parameterization for the absorption of solar radiation in the Earth's atmosphere. *J. Atmos. Sci.*, **31,** 118–133.

Pinker, R. T., and J. A. Ewing, 1985: Modeling surface solar radiation: Model formulation and validation. *J. Climate Appl. Meteor.*, **24,** 389–401.

Raschke, E., and H. J. Preuss, 1979: The determination of solar radiation budget at the Earth's surface from satellite measurements. *Meteor. Rundsch.*, **32,** 18–28.

Smith, W. L., H. M. Woolf, C. M. Hayden, D. Q. Wark and L. M. McMillin, 1979: The Tiros-N operational vertical sounder. *Bull. Amer. Meteor. Soc.*, **60,** 1177–1187.

SOLMET, 1979: Hourly solar radiation-surface meteorological observations, Volume 2, Final Report. NOAA, National Climatic Center Report TD-9724.

Tarpley, J. D., 1979: Estimating incident solar radiation at the surface from geostationary satellite data. *J. Appl. Meteor.*, **18,** 1172–1181.

Yamamoto, G., 1962: Direct absorption of solar radiation by atmospheric water vapor, carbon dioxide, and molecular oxygen. *J. Atmos. Sci.*, **19,** 182–188.